COUPLING OF THRESHOLDING AND REGION GROWING ALGORITHM FOR CHANGE DETECTION IN SAR IMAGES

Bhogendra Mishra[*] and Junichi Susaki

Department of Civil and Earth Resources Engineering, Graduate School of Engineering, Kyoto University, Kyoto, Japan

Abstract—In this research paper, we propose supervised and unsupervised change detection methodologies focused on the analysis of multitemporal Synthetic Aperture Radar (SAR) images. These approaches are based on three main steps: (1) a comparison of multitemporal image was carried out by normalized difference ratio (NDR) operator; (2) implementing a novel supervised or unsupervised thresholding and (3) generating the change map by coupling of thresholding along with a region growing algorithm. In the first step, two filtered multitemporal images were used to generate NDR image that was subjected to analysis. In the second step, by assuming a Gaussian distribution in the no-change area, we identified the pixel range that fits the Gaussian distribution better than any other range iteratively to detect the no-change area that eventually separates the change areas. In the supervised method, several sample no-change pixels were selected and the mean (μ) and the standard deviation (σ) were obtained. Then, $\mu \pm 3\sigma$ was applied to select the best threshold values. Finally, a traditional thresholding algorithm was modified and implemented with the coupling of the region growing algorithm to consider the spatial information to generate the change map. The Gaussian distribution was assumed because it better fits the conditional densities of the no-change class in the NDR image. The effectiveness of the proposed methods was verified with the simulated images and the real images associated with geographical locations. The results were compared with the manual trial and error procedure (MTEP) and traditional unsupervised expectation-maximization (EM) method. Both proposed methods gave similar results with MTEP and significant improvement in Kappa coefficient in comparison to the traditional EM method was found in both geographical locations.

* Corresponding author: Bhogendra Mishra (mishra.bhogendra.46c@st.kyoto-u.ac.jp).

The coupling of the modified thresholding with the region growing algorithm is very effective with all methods.

1. INTRODUCTION

Southeast Asia is a home of nearly 600 million populations and lies three out of thirty mega cities in the world. The region has experienced rapid urbanization with above 3% of annual growth rate for the last couple of decades and is expected in the future as well. Development associated with urbanization not only decreases the proportion of agricultural land, forest, open space and other land cover types but also affects the local as well as global environments. Therefore, change detection in multi-temporal images has attracted increasing concern, especially in environmental monitoring, land-use/cover dynamics, disaster assessment, infrastructure planning and development etc. Space borne sensor images have been extensively used to provide up-to-date land cover (LC) maps [1] economically. The use of optical images has become widely acceptable for land use/cover change detection [1], but cloud cover is a common problem of visible and infrared remotely sensed images in humid tropical region. As an alternative, Synthetic Aperture Radar (SAR) images will be the best choice in the Southeast Asia.

SAR images have already attracted great attention in the remote sensing community with its all-time, all weather capacity [2]. In the context of SAR image analysis, the problems of change detection are de-speckling, change image generations from multi-temporal images, optimum thresholding, and inclusion of spatial information etc. Several methodologies are found in the literature for change detection using SAR images. Most of them started from generating the change image using multi-temporal intensity or amplitude images [3–5]. They then used the supervised or unsupervised thresholding algorithm to segment the change and no-change areas but very few works have been done by including spatial information in the SAR change detection when moderate to low resolution images are used.

Rignot and Van Zyl in [6] suggested comparing two multi-temporal SAR images using a ratio operator. They also suggested that the ratio operator would be more effective in minimizing the speckle noise. A few other similar papers [5–7] also recommended the ratio method, which is sensitive to the presence of image speckles in the scene. Paper [3] implemented controlled adaptive iterative filtering and comparing the multi-temporal images using the log-ratio operator; finally an Expectation-Maximization (EM) thresholding algorithm was implemented. Paper [5] examines the effective methods for urban

change detection using multi-temporal space borne SAR images. They used the modified ratio operator with an EM thresholding algorithm for automatic classification of the change image into two classes, viz., change and no-change. They concluded that the change detection accuracy obtained using the modified ratio operator and Kittler-Illingworth algorithm depended on how the assumed conditional class density function fits the histogram of change and no-change classes [5]. In another work, the difference of backscattering coefficients of the pre and post events and correlation coefficients between the pre and post events were implemented. A manual trial and error method was used to obtain the appropriate threshold value to detect the change in both indicators [8].

Most of the above thresholding algorithms are applicable to bi-level thresholding [2, 3, 9, 10]. The histogram of the image is assumed to have one valley between two peaks. The peaks represent the background and objects, respectively [11]. They identified the threshold value using certain statistical criteria such as variance, mean etc. As land cover/use nature is dynamic with time, some areas have increased backscattering intensity, whereas others have a decreased intensity. Therefore, the histogram of the change image has at least two valleys and three peaks, and often the middle peak (around 1 in the case of the ratio operator) represents the no-change area. The remaining two peaks represent the change area for the increase and decrease in backscattering intensity. Thus, in land cover change, a tri-level thresholding is required, i.e., two threshold values, one segments the increase in the intensity whereas the other segments the decrease in intensity, from the no-change pixels.

Some very good unsupervised methods to obtain two-way thresholding are also available; however, they work under the assumption of same distribution in the change and no-change areas of the change image [5, 12]. Paper [12] proposes an algorithm under the Generalized Gaussian distribution in the change and no-change areas. Similarly, paper [5] evaluates the goodness of fit for several distributions. A threshold value was obtained using the EM thresholding and managed to discriminate the increase and decrease intensity areas. However, the same distribution in both the change and no-change areas may not be valid in all cases. Thus, the most important lack here is the absence of any technique that can give two thresholds to segment all the possible cases of change in the SAR images, when the change and no-change areas have different distributions.

Regarding the supervised thresholding methods, the manual trial and error procedure (MTEP) is the only popular method [1, 13]. A log-

ratio operator was implemented to generate a change image followed by adaptive filtering, and manual selection of the decision threshold for change detection was presented in [13]. In another paper [8], MTEP was implemented to obtain the appropriate threshold for detection of the change area by using the difference of backscattering coefficients between the pre and post event images. Similarly, METP has been used as the base method to compare the outcome of the proposed two-way unsupervised thresholding method in [12].

Pixel wise change detection methodologies based on the threshold value(s) only uses the spectral information of the pixel [2–5 and many others]. It mostly ignores the spatial context, and it is almost impossible to segment it with specific threshold value into the change and no-change areas perfectly. Therefore, it is very important to extend the methodology to include spatial information as well. However, thus far, spatial information is used in common practice, only in high resolution (HR) or very high resolution (VHR) images, although it is gaining popularity in image segmentation and change detection [14–16]. Several objects based change detection techniques which considered spatial information were discussed in [16]. Most of the segmentation approaches were grouped into either boundary or edge-based (discontinuity of pixels) or area-based (similarity of pixels) techniques. Another work [14] introduced a change detection model based on the Neighborhood Correlation Image (NCI). However, in the middle to low resolution of SAR images, these methods are not in practice. Although it is very difficult to implement the object based contextual information in such resolution, it may be possible to introduce the spatial consideration which can improve the change detection performance.

Thus, the major objective of this study is to investigate multitemporal single channel, single polarization Synthetic Aperture Radar (SAR) images for change detection using supervised and unsupervised change detection methods, without considering any predefined distribution in the change area. And, the spatial information will also be used to improve the change detection performance in the SAR images through the coupling of modified thresholding and region growing algorithms.

2. METHODOLOGY USED

The framework of the change detection methodology in multi-temporal SAR images is presented in Figure 1. The details regarding the methodology are presented in the following sections.
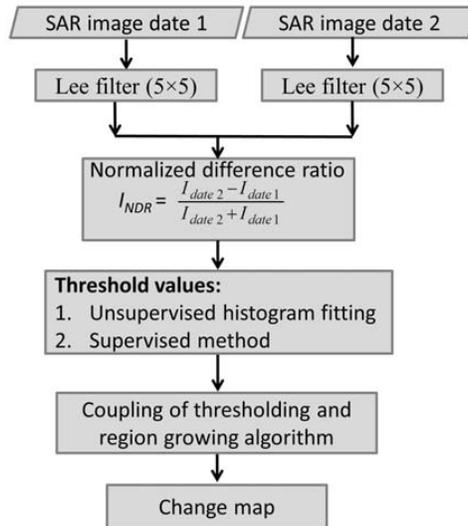
Figure 1. Work flow diagram.

2.1. Preprocessing

All images were geocoded and co-registered to the Universal Transverse Mercator (UTM) system using the Global Digital Elevation Model (GDEM) with 30 m pixel spacing. Only the amplitude of the HH component of the multi-temporal fully Polarimetric Synthetic Aperture Radar (PolSAR) images acquired by ALOS PALSAR was used for the experiment.

The multiplicative nature of speckle noise presence in the SAR image may affect the performance of the methodology. Therefore, Enhanced Lee filter of window size 5×5 was implemented to reduce the speckle noise [17]. The window size was selected with a caution, if the size is bigger the spatial resolution will lose and if the window size is smaller, the filter will not be effective.

2.2. Change Image Development

A normalized form of a ratio operator, Normalized Difference Ratio (NDR) operator, will be used to generate the change image. Unlike the ratio operator, the NDR operator generates pixel value from -1 to $+1$. All no-change pixels are clustered around 0, while all the change pixels are either close to -1 or $+1$. Therefore, it will give a clear peak for each type. More importantly, the NDR operator is effective to
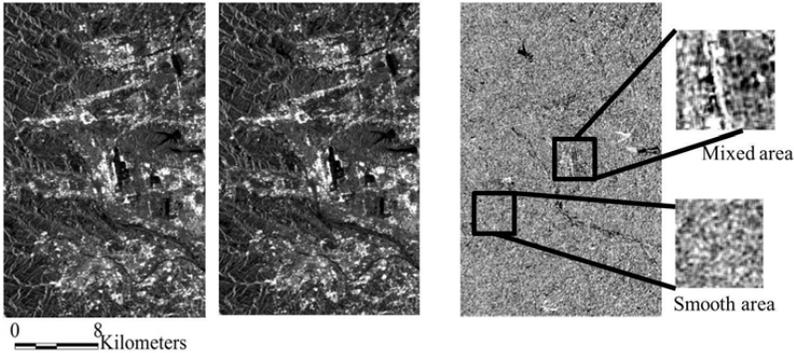
Figure 2. HH component of PolSAR images taken in 2007 and 2010, Change image (right big) generated using the NDR operator, along with the smooth area and mixed area.

generate relative changes in the multi-temporal images. The change image generated by NDR operator can be seen in Figure 2. The NDR operator is defined as:

$$Change_{i,j} = \frac{X_{2_{i,j}} - X_{1_{i,j}}}{X_{2_{i,j}} + X_{1_{i,j}}} \tag{1}$$

where $X_1 = \{X_1, i, j; \ i = 1, \ldots, m; \ j = 1, \ldots, n\}$ and $X_2 = \{X_2, i, j; \ i = 1, \ldots, m; \ j = 1, \ldots, n\}$ are co-registered images acquired on two dates, and i and j are the X and Y coordinates of pixels in the images.

To confirm the effectiveness of the NDR operator over widely used ratio operator, a following separability index is used [18].

$$Separability\_index = \frac{|\mu_c - \mu_{uc}|}{\sigma_c + \sigma_{uc}} \tag{2}$$

where μ_c and σ_c are mean and standard deviation of change class and μ_{uc} and σ_{uc} are mean and standard deviation of no-change class respectively.

The higher value of separability index implies the better separability of change area from the no-change area.

2.3. Change Mapping

We aim to classify the area into $\{C_i, C_{nc}, C_d\}$ by threshold values t_1 and t_2, where C_i, C_{nc} and C_d are associated with increase intensity, no-change and decrease intensity pixels respectively. Most of the

thresholding algorithms are based on parametric approaches that assume a predefined statistical model in all change and no-change classes [2, 3, 5, 10, 12]. But, due to the dynamic behavior of the changing area and its complex nature, assuming a predefined statistical model for change class may not be valid in all cases.

Thus, assuming a Gaussian distribution in the no-change class, and both change — increase and decrease intensity areas do not follow any distribution, two thresholding methodologies — supervised and unsupervised are proposed in this study and explain as follows.

2.3.1. Thresholding

2.3.1.1 Unsupervised Thresholding

Let the pixels in the change image be represented by the L gray levels $[0, 1, 2, \ldots, L]$. Let x_j denote the number of pixels with the gray level j. A histogram $H(x)$ is formed of the image results in an ordered set of discrete values $x_1, x_2, x_3, \ldots, x_L$. Our aim is to distinguish the $H(x)$ into three classes as follows,

$$H(x) = \sum_{j=0}^{t_1} H(x_j) + \sum_{j=t_1+1}^{t_2} H(x_j) + \sum_{j=t_2+1}^{L} H(x_j) \tag{3}$$

where t_1 and t_2 are the two thresholds that cover the no-change area. The first region from 0 to t_1 represents the change area — decrease in intensity, and the third term from t_{2+1} to L is also the change area — increase in intensity. The no-change area follows the Gaussian distribution; thus we can approximate as below.

$$\sum_{j=t_1}^{t_2} H(x_j) \approx \frac{1}{\sigma\sqrt{2\pi}} \int_{t_1}^{t_2} e^{-\frac{(x-\mu)^2}{2\sigma}} dx \tag{4}$$

where, μ and σ are the mean and standard deviation of $H(x)$ in an interval between t_1 and t_2.

Hence, the t_1 and t_2 can be found iteratively in such a way that the pixels within the range better approximate the normal distribution than any other interval in the histogram.

As shown in Figure 3, the distributions of no-change class and change classes usually overlap. Thus, the optimum threshold is often located at the point where two distributions cross each other. If t_1 and t_2 are two cross point in left and right side of no-change class, the probability density fitting of no-change class will be the best in the range from t_1 to t_2. But, if t_1 moves left, the left tail will be heavier and if it moves right, the left tail will be shorter than the ideal one and

vice versa while moving t_2. As a result, the probability density fitting will not be as perfect as before, thus this method is likely to select the cross point as the left and right bounds of the no-change area that eventually works as the threshold value.

2.3.1.2 Supervised Thresholding

It is easy to recognize the no-change area in the image with the visual interpretation, which is relatively smooth. This is a good prospect to separate the no-change area in the image. The smooth area is defined as follows.

If the pixel(s) does not have any change, ideally the pre-event and post-event images should have the same backscattering intensity. However, due to phonological changes or some noises, the backscattering intensity varies slightly; still they have a similar level of intensity. Therefore, the NDR generates a pixel value close to 0 for the no-change area and that looks smoother than other areas. The smooth area can be seen in Figure 2.

Several sample no-change clusters in the change image generated through NDR operator can be selected interactively. As, the pixels in the no-change area are normally distributed, $\mu \pm 3 \times \sigma$ can cover 99.7% of the total population and that can work as a threshold value to separate no-change area from change. Thus, if sample no-change area gives the mean (μ) and standard deviation (σ) for no-change area, the threshold values can be computed as follows.

$$\text{Threshold} = \begin{cases} \text{left Threshold } (t_1) = \mu - 3 \times \sigma \\ \text{right Threshold } (t_2) = \mu + 3 \times \sigma \end{cases} \quad (5)$$

2.3.2. Coupling of Thresholding and Region Growing Algorithm

If the change pixels have significant differences in the backscattering intensity, those pixels are located in the extreme area, near -1 or $+1$, of the histogram. However, in the boundary line of the change region, the change in the backscattering intensity may not alter significantly; therefore, those pixels are located in and around the threshold values. Such pixels are always at risk to misclassify using only the thresholding criteria. This fact is evident in Figure 3. Therefore, the classification scheme has been modified to use the spatial relationship of confirmed change and no-change pixels with those at risk. The methodology is modified by including the spatial information to detect the change area as follows.

If we have mean (μ) and standard deviation (σ) within the threshold values t_1 and t_2, the pixels less than $t_1 - \sigma$ are classified as
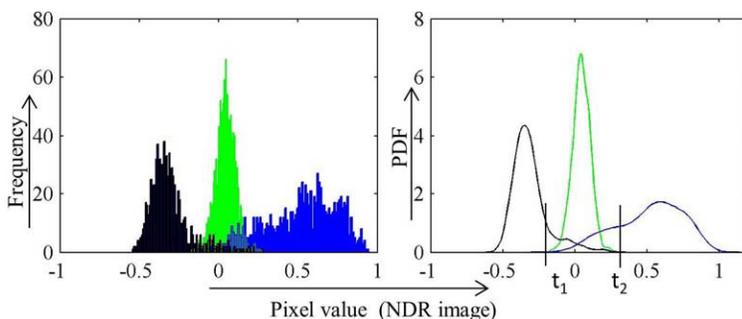
Figure 3. Histogram and non-parametric density fitting left peak — decrease intensity, middle peak — no change and right peak — increase intensity.

a change — decrease intensity (C_1). Similarly, the pixels in the range $t_1 + \sigma$ to $t_2 - \sigma$ are classified as the no change area (C_2) and greater than $t_2 + \sigma$ are classified as a change — increase intensity (C_3). These classes have very few chances to misclassify. The remaining pixels from $t_1 - \sigma$ to $t_1 + \sigma$ and $t_2 - \sigma$ to $t_2 + \sigma$ are left unclassified. The region growing algorithm [19] is then adopted to classify those unclassified pixels as.

At this stage, we have three classes (C_1, C_2, and C_3) and unclassified pixels. The classified pixels (C_1, C_2, and C_3) with modified thresholding values are treated as seed pixels. The set of unclassified pixels which have classified neighbors are defined as:

$$U = \left\{ x \notin \cup_{i=1}^{3} C_i \,|\, x \in \cup_{i=1}^{3} C_i' \right\} \qquad (6)$$

where, $i = 1, 2, 3$ for potential three classes, C_i is a set of pixels classified as i-th class, and C_i' is a set obtained by two-time dilation of C_i.

$\forall x \in U$, compute the distance (Δx_i) with each connected class as follows:

$$\Delta x_i = |g(x) - g_i(c)| \qquad (7)$$

where, $i = 1, 2, 3$, $g(x)$ is the pixel value and $g_i(c)$ the average pixel values for each class, calculated from two time dilation of considered pixel x.

A pixel will be assigned to the class which has the minimum distance from the pixel. The process will be repeated as long as there is an unclassified pixel with at least two neighboring classes. The rest of the pixels were classified as no change.

2.4. Accuracy Assessment

A confusion matrix has been used to estimate the change detection accuracy that allocates the change and no change class [20]. A confusion matrix has been developed through a cross tabulation of the results obtained from remote sensing with a corresponding ground reference dataset that gives the change detection accuracy [21]. The entries in the confusion matrix along with the associated reference values may be used to derive the numerous summary measures of the accuracy of the classes and the amount of change that has occurred. Particularly, in this study, the considered accuracy measures are correctly detected increasing and decreasing intensity (%), false alarm (%) that gives the number of missing pixels and falsely classified pixels in each class, and Kappa coefficient gives the overall accuracy. To assess the accuracy, Advanced Visible and Near Infrared Radiometer type-2 (AVNIR-2) images acquired on nearly the same date as the SAR images as well as high-resolution QuickBird images from Google Earth were used. The reference change area was acquired by manual analysis.

3. DATA USED AND STUDY AREA

A pair of simulated SAR images and two pairs of real images — associated with geographical locations in Southeast Asia — Ho Chi Minh City and Bangkok were subjected to evaluate the robustness of the proposed methodologies. The details of all data sets and study area are presented in the following sections.

3.1. Simulated Dataset

To confirm the algorithm, a simulated SAR image is considered. As the study focuses on urban change detection, a pair of simulated images represents the change in dihedral structures mainly construction, and destruction of the structures for L-band is considered. The size of the simulated image is (400×200) pixels. A SAR simulator was developed in Matlab based on the radar image formulation mechanism [22].

3.2. Ho Chi Minh City Dataset

The first real dataset in this experiment is a section of $(636 \times 1357$ pixels) two Advanced Land Observing Satellite (ALOS) Phased Array type L-band Synthetic Aperture Radar (PALSAR) images in Ho Chi Minh City acquired in April, 2007 and April, 2011. Ho Chi Minh City is one of the fastest growing Asian cities. The total population was 7.52 million in 2011 whereas in mid-2007, the city's

population was 6.65 million with nearly 3.1% of increasing rate [23]. Major changes in this section of the city are huge urban expansion in an agricultural land and deforested area. All data sets used in the study have the same acquisition parameters with the same viewing configuration. Therefore, we can assume that differences in the images' are directly related to the changes that occurred to the ground scatters.

3.3. Bangkok Dataset

The second dataset represents a section of $(548 \times 876$ pixels) two SAR images acquired by the ALOS PALSAR over Bangkok, Thailand, in May, 2009 and May, 2010. Bangkok is a mega city having 14.6 million populations with annual growth of 0.9% [23]. The image contains the majority of the highly populated urban area, thus there are not big change clusters. Similar to the Ho Chi Minh City, all data sets used in the study have the same acquisition parameters with the same viewing configuration. Therefore, we can assume that differences in the images' are directly related to the changes that occurred to the ground scatters.

4. EXPERIMENTAL RESULTS AND DISCUSSIONS

Three different experiments were performed to evaluate the results obtained from the proposed supervised and unsupervised algorithms. First, the effectiveness of the algorithm was validated in a simulated SAR image then implemented into two real images associated with geographical locations. In the geographical locations, one is the fastest growing South East Asian city — Ho Chi Minh City, and another is a Southeast Asian mega city – Bangkok. To reduce the speckle noise, a Lee filter [17] of window size 5×5 was implemented. Then, the change image was generated, and the methodologies proposed were implemented. Goodness of fit test was performed to confirm the distribution of the change image in all cases. Three statistical models, namely normal, logistic and student's-t distribution, were selected to perform the goodness of fit test. A widely used visual interpretation technique named QQ-plot was selected to confirm the goodness of fit [24]. The coupling of thresholding and region growing algorithm was done to consider the spatial information while classifying. The results were evaluated with the referenced change map developed interactively with several high and very high optical images. The accuracy measures considered are correctly detected change (%) in increase and decrease intensity area separately, false alarm (%), and Kappa coefficient. Finally, the results obtained were compared with the results obtained from the widely used EM based thresholding algorithm [2, 5, 12] and a

manual trial and error procedure (MTEP) [1, 12].

4.1. Experiment with Simulated Image

4.1.1. Statistical Analysis

To confirm the statistical distribution, samples were taken for change, no-change and mixed (change and no-change) areas from the change image generated by the NDR operator in simulated image. Figures 4(a)–(c) show the QQ-plot of the mixed, both change and no-change areas against the standard normal, logistic and student's-t distribution sample dataset. The no-change area has good alignment with all distributions; however, all other areas — both changes and all areas do not reveal any matching. If we further evaluate the matching of no-change area, normal distribution is close to impeccable in comparison to other two distributions.

To further confirm the distribution, Figures 4(d)–(f) represent the QQ-plot of optimum threshold value, narrower and wider than optimum against standard normal, logistic and student's t distribution respectively. The pixels in the optimum threshold range show the best matching against the normal distribution. The optimum threshold values were obtained with the MTEP, which gives the best results.

4.1.2. Change Mapping

The changed results obtained from simulated dataset are presented in Figure 5. The threshold values obtained by supervised and MTEP were the same, thus both of them depict the same results. The unsupervised approach has some missing alarm; however, this is recovered while implementing the coupling of thresholding and the region growing algorithm. The effect is clearly visible in the increased intensity rectangle which is smoother in the edge in comparison to that obtained only with threshold values. Some missing alarm is visible in the boundary region of all shapes in the results obtained from the EM method, which is also improved greatly while implementing the coupling of thresholding and region growing algorithm.

Table 1 represents the accuracy obtained from the simulated image with different methodologies. Increase intensity and decrease intensity show the percentage of correctly classified pixels in an increase and decrease intensity area, respectively. False alarm denotes the percentage of falsely classified pixels, and Kappa coefficient shows the overall accuracy. As the threshold value obtained from MTEP and the supervised algorithm are the same, the results from these two methods are the same. The overall performance is very high in these methods;
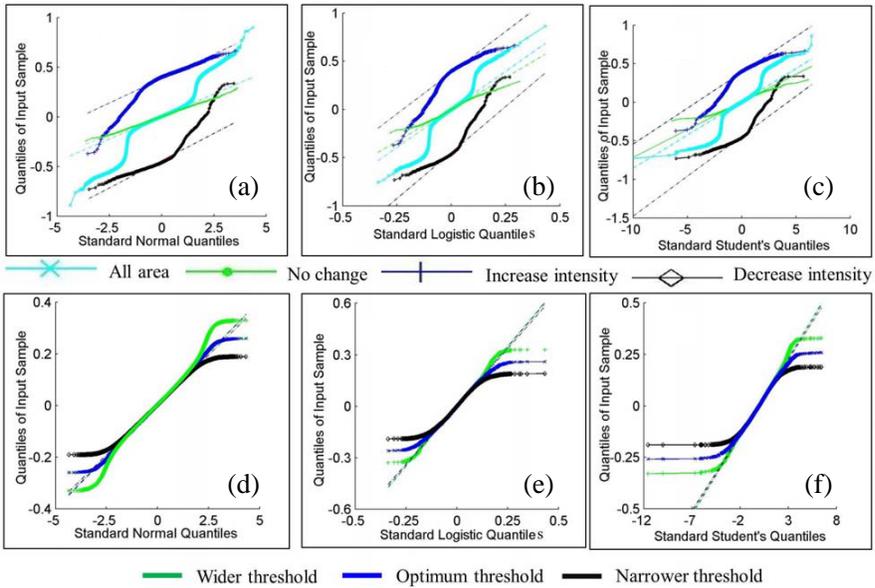
Figure 4. *QQ* plot for several input samples with various statistical distributions in simulated image.

however some overestimation causes a slight decrease in overall performance and increase false alarm. On the other hand, the proposed unsupervised method is slightly better at detecting the change pixels than EM; however, they have very similar overall accuracy because of the overestimation caused by unsupervised method. Despite having a very good change detection capacity in all methods, the coupling of thresholding with region rowing algorithm seems equally effective in reducing the false alarm and improving the detection capacity.

4.2. Site 1 — Ho Chi Minh City

4.2.1. Statistical Analysis

The first experiment associated with geographical location was performed in Ho Chi Minh City. The separability index was computed to demonstrate the effectiveness of the NDR operator in comparison to the ratio operator. Figure 6 represents the separability index for major change features namely bare land or agricultural land to dihedral structures, deforestation, and destruction of building etc. with no-change class while using NDR operator and ratio operator. The aim is

to discriminate the change area from no-change area; therefore all the separability indexes were measured with respect to no-change area. In all change types, the NDR image has a higher separability index than that for ratio image; therefore NDR operator would be better for the change detection.

Similar to the simulated image, the statistical distribution was confirmed for the samples taken for change, no-change and mixed (change and no-change) areas from the change image generated by the NDR operator in Ho Chi Minh City. Figure 7 shows the QQ-plot of the mixed, change and no-change areas against the standard normal, logistic and student's-t distribution sample dataset and with different threshold values. The optimum threshold value was obtained with the MTEP which gives the best results and presented in the same section.

Figure 7(a) is the QQ-plot of the quantiles of the all considered area, no-change area, and both change areas (increase intensity area

(a) Pre image   (b) Post image   (c) Change image – NDR

(d) Change image – ratio   (e) MTEP   (f) MTEP-RG

(g) Supervise   (h) Supervise-RG   (i) Unsupervised

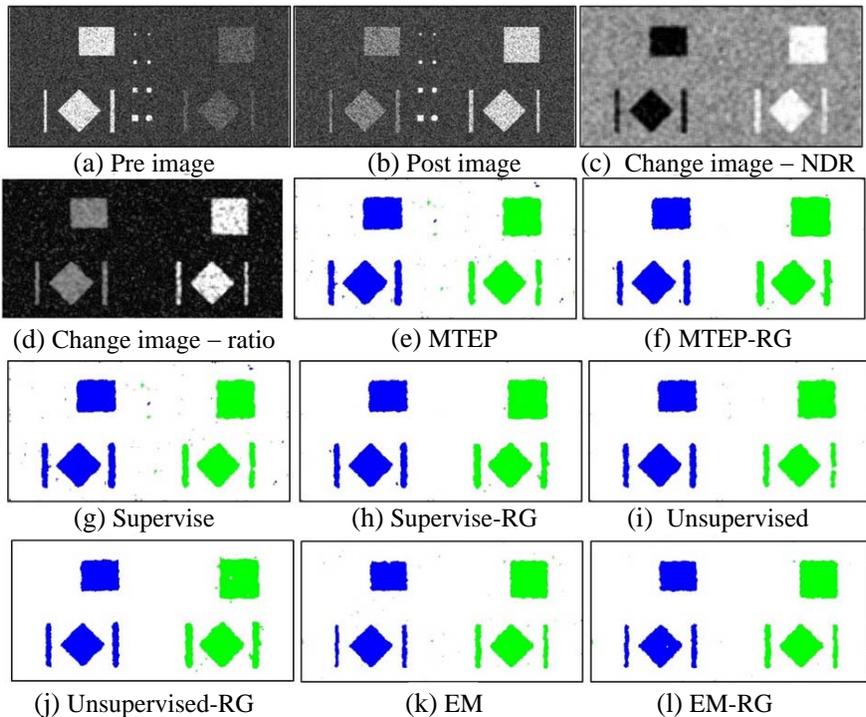(j) Unsupervised-RG   (k) EM   (l) EM-RG

Figure 5. (a), (b) Simulated SAR images, (c) NDR-image, (d) ratio-image, (e)–(l) change map obtained from several methodologies in simulated image (RG-region growing).

Table 1. Accuracy assessment in simulated data.

Indicators	MTEP	MTEP-RG	Sup.	Sup.-RG	Unsup.	Unsup.-RG	EM	EM-RG
Increase intensity (%)	91.72	95.45	91.72	95.45	90.23	93.86	88.03	93.16
Decrease intensity (%)	94.69	95.52	94.69	95.52	93.15	94.79	85.17	91.72
False alarm (%)	12.88	9.12	12.88	9.12	14.80	11.64	14.91	12.23
Kappa coefficient	0.92	0.94	0.92	0.94	0.91	0.93	0.91	0.93

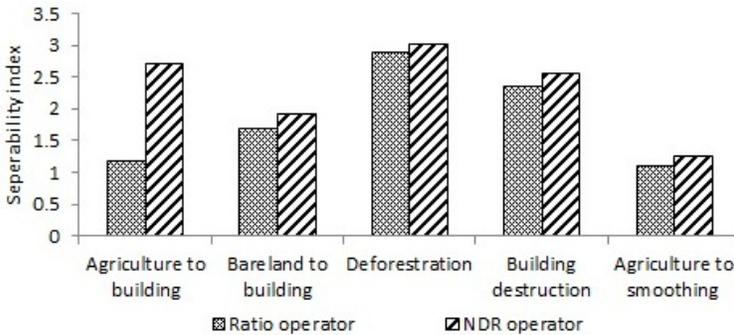Unsup. — unsupervised, Sup. — supervised, EM — expectation maximization, RG — region growing.

Figure 6. Separability index for major change classes by ratio and normalized difference ratio operator in Ho Chi Minh City.

and decrease intensity area) against the standard normal quantile. The curve for the all change area image shows a heavy tail, and the curve for the no-change area has good alignment with the reference line. However, for the change area, both the increase and decrease intensity do not reveal any match. Similar results can be seen in Figure 7(b) which is against the standard logistic quantile. Here, too, the curve for whole image reveals the long tail, and the no-change area shows a reasonable alignment with the reference logistic distribution, and no match is seen with both change areas. Figure 7(c) is for student's-t distribution with 8 degrees of freedom, which gives the best result
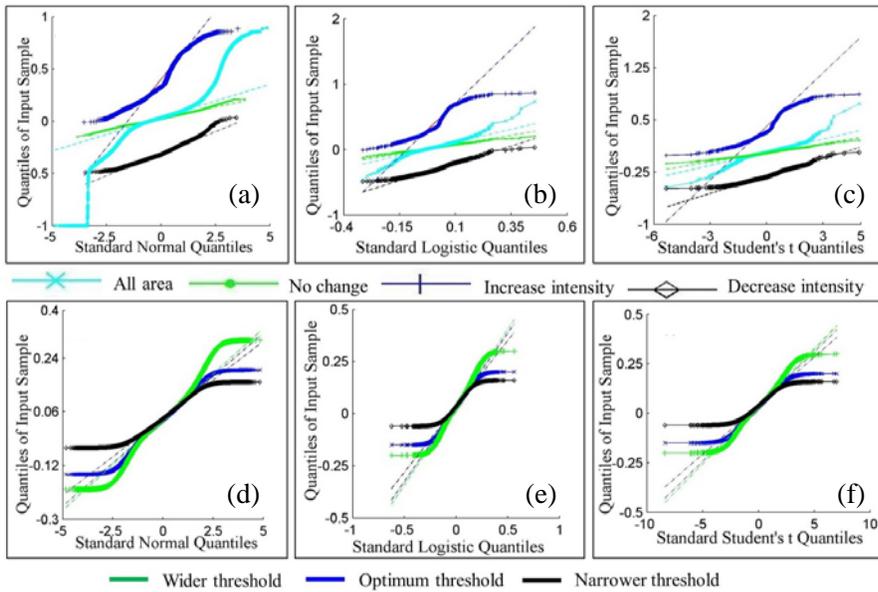
Figure 7. *QQ* plot for several input samples with various statistical distributions in Ho Chi Minh City.

compared with any other number of freedoms. Also in this case, only the no-change area has considerable alignment with the standard reference line although the matching is not as good as the normal distribution and logistic distribution. If we compare the matching in the three distributions tested in the no-change area, the standard normal quantile shows the best matching.

Based on the plotting in Figures 7(a)–(c), we conclude that the no-change area can better model with normal distribution. Still, to further improve the confidence, in Figures 7(d)–(f) we test the distribution with different threshold values in the image against all considered distributions. In Figure 7(e), two datasets, one with the optimum threshold value and the other with the narrow range, have a very short tail compared with the standard logistic distribution, and the dataset shows a wider range than the optimum having a better alignment with the standard reference line. Very similar results can be seen in Figure 7(f) as well. On the other hand, in Figure 7(d), it is clear that the wider the threshold range is, the longer the tails are, while the shorter the threshold range is, the shorter the tails are. However, if the threshold is optimum, the data can approximate with the normal distribution. It is this threshold value that gives the best

change detection results.

4.2.2. Change Mapping

The results obtained by implementing the EM, MTEP, proposed supervised, and unsupervised algorithms are presented in Figure 8, with increasing and decreasing intensity shown in green and blue, respectively.   The much the increasing intensity is changed from the open area or agricultural area to the built-up area, and the decreasing intensity area is changed from the forest to the open space (deforestation) or the agricultural area to the open space (bare land).   The main misclassification occurred in the boundary area, and the highest misclassification occurred between the no-change to the decrease intensity or vice versa. Similar kinds of misclassification are also observed in the middle part of the change area where small patches of no-change area is surrounded by the change area. These misclassifications are reduced significantly while implementing the coupling of thresholding with the region growing algorithm. Thus in the change detection problem, a threshold value alone is unlikely to give a perfect result because of the spatial relation of the pixels in the boundary region. This is confirmed by the effectiveness of the methods proposed with the inclusion of spatial information in the generation of an accurate change detection map.

Only thresholding algorithms and the coupling of modified thresholding with the region growing algorithms were implemented indepen-

Table 2. Accuracy assessment in Ho Chi Minh City.

Indicators	MTEP	MTEP-RG	Sup.	Sup.-RG	Unsup.	Unsup.-RG	EM	EM-RG
Increase intensity (%)	82.52	84.76	86.78	86.51	80.83	80.87	82.01	82.31
Decrease intensity (%)	82.39	92.69	66.70	86.81	53.13	62.75	39.08	49.09
False alarm (%)	11.00	10.25	12.32	11.13	11.87	10.30	13.12	11.43
Kappa coefficient	0.76	0.78	0.74	0.76	0.72	0.75	0.70	0.73

Unsup. — unsupervised, Sup. — supervised, EM — expectation maximization, RG — region growing.

dently. The change detection results with the coupling of modified thresholding and the region growing algorithm show significant improvement over the results obtained with only thresholding values in all considered algorithms. Additionally, the results obtained from both methodologies proposed outperform the results from the traditional EM thresholding.

Table 2 shows the accuracy assessment of the change results obtained in the Ho Chi Minh City. Similar to the previous section, the increase intensity and decrease intensity show the percentage of correctly classified pixels in an increase and decrease intensity area
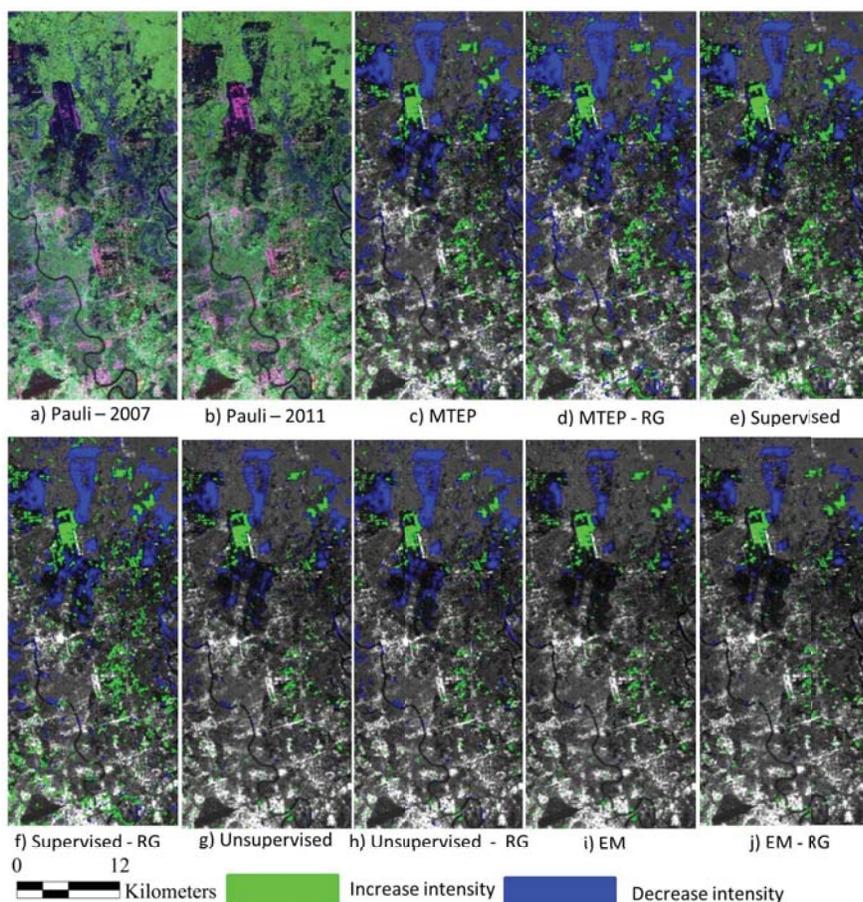

Figure 8. (a), (b) Pauli composition of PolSAR image, (c)–(j) change map obtained from several methodologies in Ho Chi Minh City.

respectively. Likewise, false alarm reflects the percentage of falsely classified pixels and Kappa coefficient shows the overall accuracy. In all indices MTEP gave the best possible result. The supervised methodology also generated similar result with the 0.75 of Kappa coefficient and 11.13% of false alarm. The coupling of thresholding with region growing algorithm appears highly effective in all cases.

The change pixels surrounded by no-change pixels, and vice versa in several places, were observed in the final results (see Figures 8(d), (f), (h), (j)) while considering the spatial information. This is because several patches within the forests were already open in the pre-image; the intensity changes in these pixels are relatively higher than others in the no-change area. This may be due to the filtering effects in the pixels surrounded by the highly varying pixel intensity or noise introduced from the surrounding area to the enclosed small area. If changes in the center really occur, the backscattering intensity should vary in the center pixels to at least as high as in the surrounding pixels, which justify them to be classified as change area. The detection of a small patch of no-change area that is surrounded by the change area is impressive.

4.3. Site 2 — Bangkok

4.3.1. Statistical Analysis

Another experiment with geographical location was performed in Bangkok. In this experiment, we considered a relatively short time interval, so it has a little change area compared with site-1. Figure 9 represents the separability index for major change features namely bare land or agricultural area to dihedral structures, deforestation, building
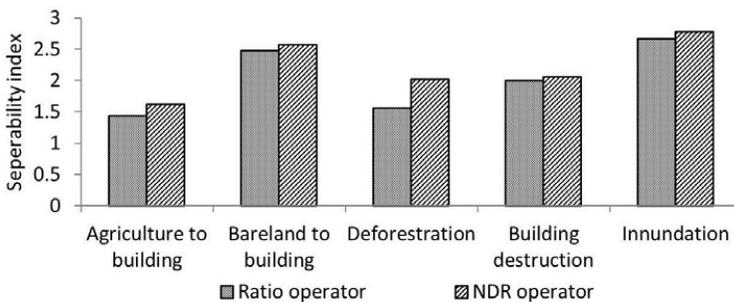

Figure 9. Separability index in several change area with respect to no change area in Bangkok.
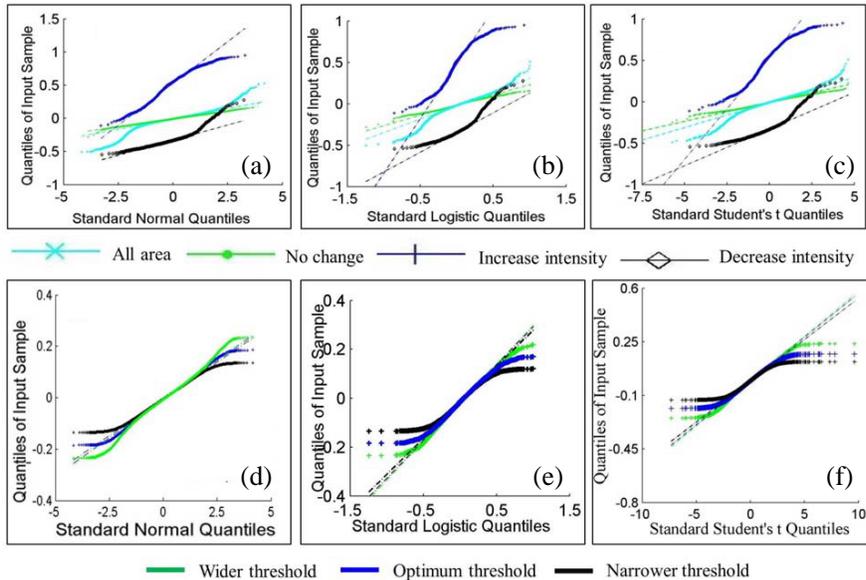
Figure 10. *QQ* plot for several input samples with various statistical distributions in Bangkok.

destruction, and an inundation area with no-change class while using the NDR operator and the ratio operator. Similar to Ho Chi Minh City, the NDR image has a higher separability index than that in the ratio image in all change classes.

Similar to the Ho Chi Minh City the statistical distribution was confirmed with the samples taken for change, no-change and mixed (change and no-change) areas from the change image generated by the NDR in Bangkok. Figure 10 shows the *QQ*-plot of the mixed, change and no-change areas against the standard normal, logistic and student's-t distribution sample dataset and with different threshold values. The optimum threshold value was obtained with the MTEP which gives the best results and presented in the same section.

Figures 10(a)–(c) represent the *QQ*-plot of the quantiles of the all considered area, no-change area, and both change areas against the standard normal quantile, standard logistic quantile and student's t-distribution quantile with 8 degrees of freedom. The nature of the curves in all distributions and in all input samples is very similar to that in simulated image and Ho Chi Minh City. The curve for all area shows a heavy tail; however, the curve for the no-change area has good alignment with the reference line. Furthermore, for the change area,

both the increase and decrease intensities do not reveal any match in all distributions. If we compare the matching in the three distributions tested in the no-change area, the standard normal quantile shows the best matching.

The change image in Bangkok area is plotted against all selected statistical distributions with optimum, narrower and wider threshold values to further improve the confidence. The plotting is represented in Figures 10(d)–(f). The nature of the plots in all threshold values in all distributions is similar to that in Figures 7(d)–(f). Thus, this test also confirms the Gaussian distribution in no-change area and eventually, the optimum threshold range as well.

4.3.2. Change Mapping

Figure 11 represents the change results obtained by implementing the EM, MTEP, proposed supervised and unsupervised algorithms in Bangkok. Similar to simulation dataset, the MTEP and supervised
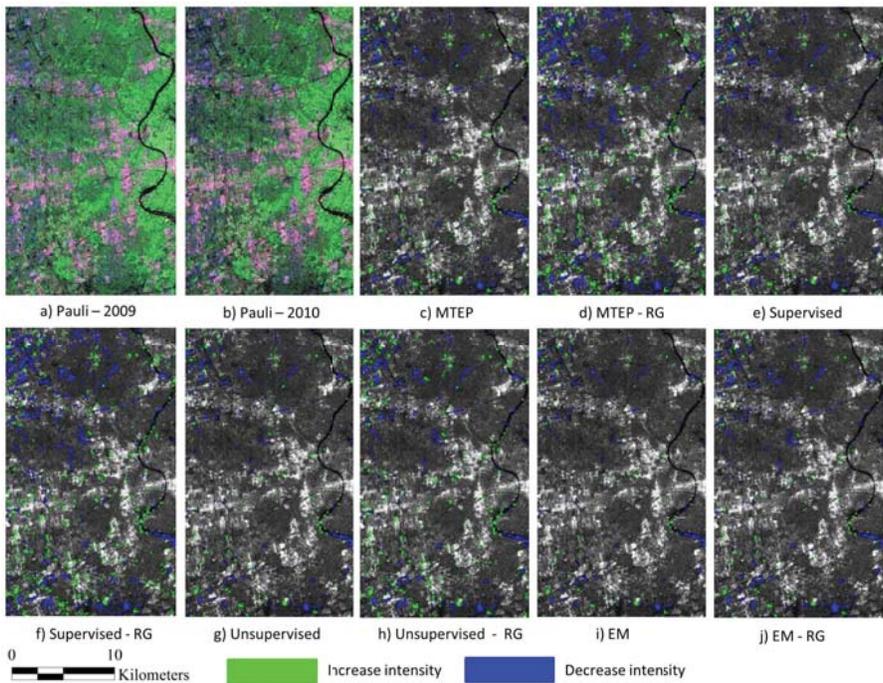

Figure 11. (a), (b) Pauli composition of PolSAR image, (c)–(j) change map obtained from several methodologies in Bangkok.

algorithms generate the same results on this site. The major changes are from open space or agriculture to built-up and inundation area. Similar to the previous experiment, the coupling of the modified thresholding with a region growing algorithm, which incorporates the spatial information, enhances the performance greatly. Concerning the change detection accuracy, the performance given by the both proposed methodologies is superior to that in EM and supervised method has similar to MTEP which is regarded as the best method.

The change accuracies obtained in Bangkok are presented in Table 3. Similar to the simulated results, the MTEP and supervised methodology have the same results followed by the proposed unsupervised methodology. The improvement in the Kappa coefficient, overall detection capability and false alarm are clear in both proposed methodologies in comparison to EM method. The improvement in correctly classifying pixels while implementing the coupling of thresholding with region growing algorithm is significant. The proposed coupling of thresholding with region growing algorithm appears more efficient in the area where higher false classification occurs.

Table 3. Accuracy assessment in Bangkok.

Indicators	MTEP	MTEP-RG	Sup.	Sup.-RG	Unsup.	Unsup.-RG	EM	EM-RG
Increase intensity (%)	78.19	78.85	78.19	78.85	64.98	73.35	52.86	61.23
Decrease intensity (%)	87.25	98.95	87.25	98.95	67.65	94.73	67.23	85.88
False alarm (%)	4.16	4.28	4.16	4.28	6.47	4.69	6.87	5.19
Kappa coefficient	0.84	0.85	0.84	0.85	0.74	0.84	0.72	0.81

Unsup — unsupervised, Sup. — supervised, EM — expectation maximization, RG — region growing.

The same kinds of misclassification can be seen in the Bangkok as in the Ho Chi Min City. Similar to the previous experiment, the accuracy of the unsupervised and supervised classification is low when the threshold values alone are used. The reason for the higher error resulting from using the threshold value alone is that the change area

may not have a clear variation in the backscattering intensity in the pre and post-event images to separate the changes. However, while implementing the coupling of thresholding with the region growing algorithm, such kinds of misclassification get reduced. And it appears extremely effective in the boundary region.

4.4. Overall Discussion

The performance of both of the methodologies proposed is higher than that obtained by using the EM under the assumption of lognormal distribution [5] and very similar to MTEP in all experiments including simulated image. The assumption of same distribution in both change area and no-change area [5, 12] may not be valid in all the cases. It depends on the change area, size, and amount of variations in the intensity and nature of the change etc. Thus, the EM method cannot give stable threshold values in different cases. In contrast to that, while using the NDR operator, the assumption of normal distribution in no-change area is rather stable. And, the methodologies proposed do not need any predefine distribution in the change area.

The coupling of the thresholding and region growing algorithm appears very effective in all experiments performed here in this paper. The accuracy obtained in simulated image is higher than that obtained in real images associated with the geographical locations; however, the pattern of the performance improvement while implementing the proposed methodologies is similar. The kappa coefficient is increased by 0.05 in the unsupervised, and 0.06 while using the supervised methodology in Ho Chi Minh City. Similarly, in Bangkok, the improvement is better than that in Ho Chi Minh City, which is improved by 0.13 in comparison to the traditional EM method.

The thresholding algorithms give a threshold value on either side of the no-change area. But these threshold values unlikely give perfect results. Therefore, inclusion of the spatial information is instrumental in improving the performance for each methodology. As in Figure 3, if we move the t_1 left, the probability to misclassify the no-change to change will decrease, but the probability to misclassify the change into no-change will be increased, and vice versa while moving it to the right side. A similar result can be seen if we move t_2 to the left or right. Therefore, the threshold value alone cannot give the best result, and coupling of thresholding with region growing algorithm is more effective if there is higher missing and false alarm in thresholding only. The methodology proposed will be a promising solution that includes the spatial information along with the thresholding. The methodologies proposed are effective in those regions where the pixels are in higher risks to misclassify, especially along the edge of the change area.

5. CONCLUSIONS

In this research, one supervised and one unsupervised change detection methodology under the mixed distribution (normal distribution in the no-change area and no assumption for the change area) with the coupling of the thresholding and the region-growing algorithm are proposed. Effectiveness of the methodologies proposed in detecting the change area was confirmed in simulated SAR images as well as real SAR images associated with the geographical locations — Ho Chi Minh City and Bangkok.

The main strengths of the proposed approaches are: 1) the change image generation through the NDR operator from multi-temporal SAR image. NDR image is characterized as a higher separability index than widely use ratio image for several change classes, they eventually improve the accuracy of the estimation of the optimum threshold, and depicts the Gaussian distribution in the no-change area, 2) both proposed thresholding methodologies are computationally easy and stable (they are independent to the distribution in the change area and the Gaussian distribution in the no-change area is rather stable), and 3) the coupling of thresholding and region growing algorithms enable to include the spatial information in the moderate to low resolution images and equally efective to both supervised as well as unsupervised thresholding algorithms.

Concerning the limitation of the methodology proposed, both methods are not able to detect the change, if it is not statistically significant. This fact is applicable to MTEP and EM thresholding as well. In the future, we intend to generalize the approach for all data types, such as optical and multi-frequencies SAR images.

ACKNOWLEDGMENT

REFERENCES

1. Lunetta, R. S., J. F. Knight, J. Ediriwickrema, J. G. Lyon, and L. D. Worthy, "Land-cover change detection using multi-temporal MODIS NDVI data," *Remote Sens. of Envt.*, Vol. 105, No. 2, 142–154, Nov. 2006.

2. Moser, G. and S. B. Serpico, "Generalized minimum-error thresholding for unsupervised change detection from SAR amplitude imagery," *IEEE Trans. Geosci. Remote Sens.*, Vol. 44, No. 10, 2972–2982, Oct. 2006.

3. Bazi, Y., L. Bruzzone, and F. Melgani, "An unsupervised approach based on the generalized Gaussian model to automatic change detection in multitemporal SAR images," *IEEE Trans. Geosci. Remote Sens.*, Vol. 43, No. 4, 874–887, Apr. 2005.

4. Liao, M., L. Jiang, H. Lin, B. Buang, and J. Gong, "Urban change detection based on coherence and intensity characteristics of SAR imagery," *Photogrammetric Engineering & Remote Sensing*, Vol. 74, No. 8, 999–1006, Aug. 2008.

5. Ban, Y. and O. A. Yousif, "Multitemporal space borne SAR data for urban change detection in China," *IEEE J. of Selected Topics in Applied Earth Observations and Remote Sensing*, Vol. 5, No. 4, 1087–1094, Aug. 2012.

6. Rignot, E. J. M. and J. J. Van Zyl, "Change detection techniques for ERS-1 SAR data," *IEEE Trans. Geosci. Remote Sens.*, Vol. 31, No. 4, 896–906, Jul. 1993.

7. Pacifici, F., F. Del Frate, C. Solimini, and W. J. Emery, "An innovative neural-net method to detect temporal changes in high-resolution optical satellite imagery," *IEEE Trans. Geosci. Remote Sens.*, Vol. 45, No. 9, 2940–2952, Sep. 2007.

8. Uprety, P. and F. Yamazaki, "Detection of building damage in the 2010 Haiti earthquake using high-resolution SAR intensity images," *J. Japan Asso. for Earthquake Engineering*, Vol. 6, 21–35, 2012.

9. Ramesh, N., J. H. Yoo, and I. K. Sethi, "Thresholding based on histogram approximation," *IEEE Proc. — Vis. Image Signal Proces.*, Vol. 142, No. 5, 271–279, Oct. 1995.

10. Kittler, J. and J. Illingworth, "Minimum error thresholding," *Pattern Recognit.*, Vol. 19, No. 1, 41–47, 1986.

11. Albregtsen, F., "Nonparametric histogram thresholding methods — Error versus relative object area," *Proc. Eighth Scandinavian Conf. Image Analysis*, 273–280, Tromso, Norway, 1993.

12. Bazi, Y., L. Bruzzone, and F. Melgani, "Automatic identification of the number and values of decision thresholds in the log-ratio image for change detection in SAR images, " *IEEE Geosci. and Remote Sens. Letters*, Vol. 3, No. 2, 349–353, Jul. 2006.

13. Dekker, R. J., "Speckle filtering in satellite SAR change detection imagery," *Int. J. Remote Sens.*, Vol. 19, No. 6, 1133–1146,

Nov. 1998.

14. Im, J. and J. R. Jensen, "A change detection model based on neighborhood correlation image analysis and decision tree classification," *Remote Sens. of Envt.*, Vol. 99, No. 3, 326–340, Sep. 2005.

15. Cannavacciuolo, L., G. Moser, W. Emery, and S. B. Serpico, "A contextual change detection method for high-resolution optical images of urban areas," *Urban Remote Sensing Joint Event*, 1–7, Apr. 2007.

16. Hussain, M., D. Chen, A. Chen, H. Cheng, H. Wei, and D. Stanley, "Change detection from remotely sensed images: From pixel-based to object-based approaches," *ISPRS Journal of Photogrammetry and Remote Sensing*, Vol. 80, 91–106, Apr. 2013.

17. Yasnoff, W. A., J. K. Mui, and J. W. Bacus, "Error measures for scene segmentation," *Pattern Recognit.*, Vol. 9, No. 4, 217–231, 1977.

18. Mishra, P. and D. Singh, "Land cover classification of PALSAR images by knowledge based decision tree classifier and supervised classifiers based on SAR observables," *Progress In Electromagnetics Research B*, Vol. 30, 47–70, 2011.

19. Adams, R. and L. Bischof, "Seeded region growing," *IEEE Trans. on Pattern Analysis and Machine Intelligence*, Vol. 16, No. 6, 641–647, Jun. 1994.

20. Congalton, R. G. and K. Green, *Assessing the Accuracy of Remotely Sensed Data: Principals and Practices*, CRC Press, 2009.

21. Foody, G. M., "Accessing the accuracy of land cover change with imperfect ground reference data," *Remote Sens. of Envt.*, Vol. 114, No. 10, 2271–2283, Oct. 2010.

22. Inglada, J. and G. Mercier, "A new statistical similarity measure for change detection in multitemporal SAR images and its extension to multiscale change analysis," *IEEE Trans. Geosci. Remote Sens.*, Vol. 45, No. 5, 1432–1445, May 2007.

23. World Population Prospects, The 2012 Revision, United Nations, New York, 2012.

24. Helsel, D. R. and R. M. Hirsch, *Statistical Methods in Water Resources Techniques of Water Resources Investigations*, Book 4, Chapter A3, US Geological Survey, 2002.